Luz Minguez, I.; Roesler, C.; Epp, K.; Llabrés I Xamena, FX.; Fischer, RA. (2015). Pd@UiO-66-Type MOFs Prepared by Chemical Vapor Infiltration as Shape-Selective Hydrogenation Catalysts. European Journal of Inorganic Chemistry. 23:3904-3912. doi:10.1002/ejic.201500299

Pd@UiO-66-type MOFs Prepared by Chemical Vapor Infiltration as Shape-selective Hydrogenation Catalysts

I. Luz,[a] C. Rösler,[b] K. Epp,[b] F. X. Llabrés i Xamena,*[a] and R. A. Fischer*[b]

[a] Instituto de Tecnología Química, Universidad Politécnica de Valencia, Consejo Superior de Investigaciones Científicas, Avenida de los Naranjos s/n, 46022 Valencia (Spain), E-mail: fllabres@itq.upv.es URL: http://personales.upv.es/fllabres

[b] Chair of Inorganic Chemistry II, Ruhr-University Bochum Universitätsstrasse 150, 44801 Bochum (Germany), E-mail: roland.fischer@ruhr-uni-bochum.de

Abstract: Host-guest inclusion properties of UiO-66 and UiO-67 metal organic frameworks have been studied using ferrocene (FeCp2) as probe molecule. According to variable temperature solid state 1H and 13C CP-MAS-NMR, two different environments exist for adsorbed FeCp2 inside UiO-66 and UiO-67, which have been assigned to octahedral and tetrahedral cavities. At room temperature, a rapid exchange between these two adsorption sites occurs in UiO-67, while at -80ºC the intracrystalline traffic of FeCp2 through the triangular windows is largely hindered. In UiO-66, FeCp2 diffusion is already impeded at room temperature, in agreement with the smaller pore windows. Palladium nanoparticles (Pd NPs) encapsulated inside UiO-66 and UiO-67 have been prepared by chemical vapor infiltration of (allyl)Pd(Cp) followed by UV- irradiation. Infiltration must be carried out at low temperature (-10 ºC) to avoid uncontrolled decomposition of the organometallic precursor and formation of Pd NPs at the external surface of the MOF. The resulting Pd-MOFs are shape selective catalysts, as shown for the hydrogenation of carbonyl compounds with different steric hindrance.

Introduction

Metal Organic Frameworks (MOFs) are a class of crystalline porous materials constructed by metal ions or metal oxo-clusters connected through multidentate organic ligands into extended mono-, bi- or tridimensional frameworks. With a strictly regular and tunable pore system and surface areas of thousands of square meters per gram, MOFs may play a relevant role in future catalysis,[1-4] gas separation/storage[5, 6] and sensing applications.[7] In particular, the huge space available for encapsulating catalytic species offers a means for preparing MOF-based heterogeneous catalysts, in such a way that the exogenous catalytic species encapsulated inside the pores of the MOF can be effectively dispersed to avoid aggregation or mutual interference or deactivation.

To date, examples of successful encapsulation inside MOFs include the preparation of metal (Pd, Pt, Au, Ru, etc)[8-12] and metal oxide (ZnO, TiO2, etc)[13, 14] nanoparticles (NPs), as well as molecular (discrete) species (phthalocyanines, polyoxometalates, salen complexes, etc). In particular, preparation of metal NPs encapsulated in MOFs (Metal@MOF) has attracted much interest in recent years due to the potential of these composite materials in heterogeneous catalysis, as well as adsorption, gas storage and optoelectronic applications. The general method for preparing these compounds usually start with the inclusion of suitable metallic precursors within the pores of the MOF material, either by impregnation with a liquid solution of the precursor or by chemical vapor infiltration. Irrespective of the method used, loading of the precursor is followed by the controlled decomposition/reduction by thermal treatment or UV irradiation, giving rise to metal NPs. Alternative methods for preparing Metal@MOFs involve

assembling the MOF around pre-formed metal NPs.[15] Ideally, the metal NPs formed should be occluded inside the pores and their dimensions should not exceed those of the accommodating cavity. However, depending on the preparation method and the particular conditions used, formation of (large) metal NPs at the external surface, together with partial destruction of the MOF skeleton, can take place, which largely complicate the possibility to develop shape-selective processes as well as other applications requiring highly monodisperse metal NPs.

Early work on Metal@MOF systems reported mainly the use of MOF-5 and HKUST-1 as hosts, while later studies focused on more thermally and chemically stable MOFs, such as those of the MIL[16] and ZIF[8] families. Catalytic activity of the resulting Metal@MOFs has been demonstrated for several reactions, including hydrogenation and epoxidation of olefins, alcohol and aldehyde oxidation, CO oxidation, nitroaren reduction, C-C coupling reactions (Suzuki-Miyaura, Heck, Sonogashira, Ullmann), synthesis of methyl isobutyl ketone, etc. However, the results obtained in most cases indicate that encapsulated metal NPs have only modest activities. This is not surprising after all, since in most cases the use of MOF as support does not introduce any benefit to the catalytic process, but rather it may increase diffusion limitations of the reaction substrates and products. Therefore, it is by far more interesting to apply these Metal@MOFs to reactions in which the MOF participates actively, by introducing additional active centers (located at their metallic or organic components) which, when combined with the encapsulated species, lead to multifunctional solids that can catalyze multistep tandem reactions or they can act synergetically through dual activation of the reaction substrates. A couple of examples already exist on the preparation of multifunctional catalysts based on Metal@MOFs, some of them reported recently by our group. Thus we have demonstrated that Pd@MIL-101 combined hydrogenation properties of the encapsulated Pd NPs and Lewis acid character of the Cr3+ metallic nodes into a bifunctional catalyst for the one-pot sequential transformation of citronellal to isopulegol (acid catalyzed isomerization) and isopulegol to menthol (hydrogenation of C=C bond).[17] Analogously, we also showed that combination of metal-acid properties of Pd@MIL-101 and Pt@MIL-101 allows performing multi-step tandem reactions based on reductive amination of carbonyl compounds for the preparation of secondary amines and N-containing heterocycles.[18] Alternatively, the chemical environment inside the pore system of the MOF, along with long-range interactions and confinement effects imposed by the framework, can modulate the catalytic properties of the encapsulated NPs, thus altering their activity and the (shape-, chemo-, enantio- or regio-) selectivity of the catalytic reaction. In this case it is evident that the metal NPs need to be located exclusively in the internal surface of the MOF, where the framework can effectively control the reaction depending on the size and shape of the substrates, products or transition states.

Among the various MOFs that a priori could be attractive supports for preparing encapsulated metal NP, UiO-66 type zirconium dicarboxylates have some remarkable advantages: i) a considerably high thermal, chemical and mechanical stability, arising from the high connectivity of the Zr6 inorganic building blocks through 12 ligands; ii) a three dimensional pore system with two types of cavities (tetrahedrical and octahedrical), both of them available for encapsulation; and iii) a high tunability of both, pore size and functionality of the ligands, either by direct synthesis or through post-synthetic modification (PSM). This allows us to introduce a large number of different catalytic active centers at the ligands, and to modify the chemical environment inside the cavities and the properties of the Zr6 clusters through resonance and electronic induction effects. The structure of UiO-type MOFs is shown in Figure 1.

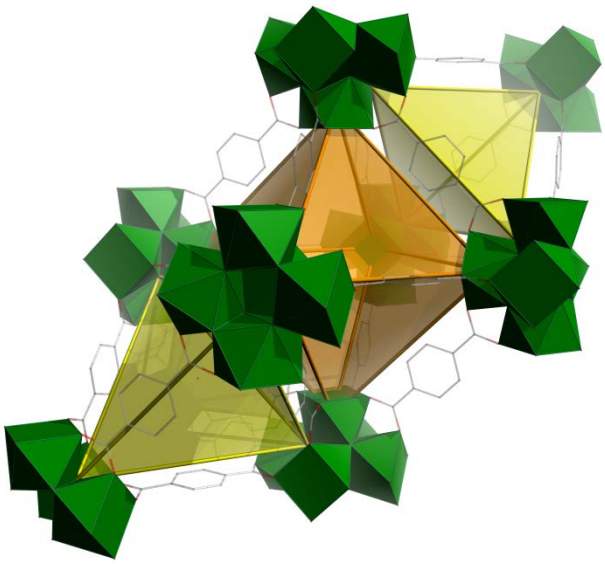

Figure 1. Structure of the UiO-type materials, revealing the Zr6 clusters (green polyhedral) as well as the octahedral and tetrahedral cavities (orange and yellow, respectively), both accessible through triangular windows. The edges of these polyhedra contain terephthalate (UiO-66) or biphenyl dicarboxylate (UiO-67) linkers.

Nevertheless, despite the high potential of UiO-type materials, the reports describing metal NPs encapsulation inside these materials are very scarce to date: only four in total, to the best of our knowledge, and all of them appeared less than one year ago. Thus, Guo et al.[19] described the synthesis of Pt@UiO-66-NH2 by impregnation of aqueous solutions of K2PtCl4 followed by reduction at 473 K in a H2 flow. According to these authors, monodispersed (1.2 ± 0.2 nm) Pt NPs were prepared, with metal loadings as high as 10.7 wt% of Pt. TEM measurements with sample tilting suggested the location of the NPs inside the cavities of the MOF, which would explain the shape-selective properties of the material, as shown for the hydrogenation of various olefins of different size (ethylene, 1-hexene and 1,3-cyclooctadiene) or the chemoselective reduction of cinnamaldehyde to cinnamyl alcohol. Later,[20] the same authors combined the oxidizing properties of Pd NPs and the Lewis acidity of the inorganic building blocks of UiO-66-NH2 into a bifunctional material, Pd@UiO-66-NH2, to catalyze the conversion of benzyl alcohol to benzaldehyde followed by acetalization in a tandem process.

Zhang et al.[21] used an alternative method for preparing Pt@UiO-66, consisting in building the MOF around pre-formed Pt NPs capped with polyvinylpyrrolidone (PVP). In this way, shape-selective properties were also observed for the liquid phase hydrogenation of olefins (1-hexene, cyclooctene, trans-stilbene, triphenyl ethylene and tetraphenyl ethylene), and 4-nitrophenol reduction with NaBH4.

The last example was reported by Chen et al.,[22] using yet another different preparation strategy. These authors prepared a mixed-ligand UiO-67 material containing both, biphenyl-4,4’-dicarboxylate and the metalloligand (2,2’-bipyridin)-5,5’-dicarboxylic acid with PdCl2 coordinated to the bipyridine N atoms. Once formed the Pd-containing mixed-ligand MOFs, Pd NPs were obtained by reducing the material at 523 K in H2 for 4 h. The resulting material was used as a catalyst for olefin hydrogenation, alcohol oxidation and nitrobenzene reduction.

To date, chemical vapor deposition (CVD) or chemical vapor infiltration (CVI) of volatile metal precursors is not among the techniques used for preparing Metal@UiO-type materials, in spite of being generally accepted that (solventless) CVD methods usually leads to more homogeneous distribution of the NPs within the MOFs as compared to samples prepared by impregnation from solution. CVI also can have some advantages with respect to the encapsulation of pre-formed NPs, since the substances used in the latter method for stabilizing the NPs suspension (such as PVP) remain also entrapped inside the pore system of the MOF and may obstruct the interaction of the metal sites with the reacting substrates. On the contrary, the precursors used in CVD decompose cleanly by a thermal treatment or UV irradiation, giving rise to naked NPs in the final solid. Herein, we describe for the first time the preparation of Metal@UiO-type materials by using a CVD method, and the evaluation of the catalytic activity and eventual shape-selective properties of the resulting materials. The applicability of the synthesis procedure is demonstrated for the preparation of Pd NPs inside UiO-66 and UiO-67. Previous characterization of the host-guest chemistry (and reactivity) of the UiO materials was performed by adsorbing ferrocene, [Fe(□5-C5H5)2] (hereafter FeCp2), due to its well-known inertness and thermal and chemical stability. Moreover, the dimensions of this molecule (3.5 x 4.5 x 4.5 Å3) are close to those of the organometallic compound used as precursor of Pd NPs, (allyl)Pd(Cp), [Pd(□3-C3H5)(□5-C5H5)] (4.5 x 4.5 x 4.5 Å3), so that similar steric hindrance can be expected for both compounds.

Results and Discussion

Gas phase loading of FeCp2 into UiO-66 and UiO-67.

After loading UiO-67 with FeCp2 from the gas phase (see Experimental Section) a clear and fast color change of the solid, from white to yellowish, was appreciated. Meanwhile, the color change in UiO-66 (white to reddish) was appreciatively slower, in line with the larger pore size of UiO-67 and the less hindered diffusion of FeCp2 with respect to UiO-66. The amount of FeCp2 adsorbed on the loaded MOFs (hereafter denoted FeCp2@UiO-66 and FeCp2@UiO-67) was estimated from both the TGA curves (see Fig. S1 in Supporting Information) and elemental analysis (Zr:Fe molar ratio as determined by ICP-OES). Both techniques gave similar and consistent results for the FeCp2 loading: 19.8 wt% according to elemental analysis for UiO-66 (23 wt% according to TGA), and 45.3 wt% (50 wt% from TGA) for UiO-67. These values are also consistent with the higher pore volume of UiO-67 with respect to UiO-66 (0.994 vs 0.457 cm3g-1, as determined by isothermal N2 adsorption). According to the FeCp2 loading data, 3 FeCp2 molecules per MOF molecular formula are adsorbed in UiO-66, while up to 11 FeCp2 molecules can be accommodated in UiO-67; i.e., the materials can be formulated as (FeCp2)3@[Zr6O6(BDC)6] (UiO-66), and (FeCp2)11@[Zr6O6(BPDC)6] (UiO-67).

It is important to note that the same loading procedure used for UiO-66 and UiO-67 was also applied to UiO-66-NH2 (an isoreticular MOF in which terephthalate ligands are replaced by aminoterephthalate). However, in this case the amount of FeCp2 loaded was negligible (0.2 wt% according to the elemental analysis). This is probably due to the narrowing of the pores in UiO-66-NH2 due to the presence of –NH2 groups, which effectively prevents diffusion of FeCp2.

X-ray diffraction was used to check that the crystallinity of the MOFs was preserved during FeCp2 loading (see Figures S2 and S3 in Supporting Information). In both cases, changes were detected in the relative intensity of some of the diffraction lines, as well as a slight expansion of the cubic unit cell, from a = 20. 647(3) to 20.759(2) Å in the case of UiO-66 (expansion of +5.4%), and from a = 26.677(3) to 26.813(4) Å in the case of UiO-67 (expansion of

5.1%). The presence of FeCp2 in the UiO-loaded samples was confirmed by FTIR: New bands appear at 1097, 995 and 808 cm-1 (symmetric and asymmetric C-C stretching, C-H rocking and perpendicular bending of C-H bonds, respectively), as well as a complex band around 3050 cm 1 due to C-H stretching. These bands are absent in the spectra of as-prepared UiO-66 and UiO-67 (see Fig. S4 in Supporting Information). Meanwhile, minor changes are observed in the IR absorption bands characteristic of the pristine MOFs, which are more evident in the case of UiO-67. In particular, a bathochromic shift of both asymmetric and symmetric O-C-O stretching modes is observed, from 1590 to 1578 cm-1 and from ~1390 to ~1370 cm-1 (in the case of UiO-66, the shifts are smaller), probably reflecting that some local distortion of the [Zr6O6] building units is produced upon FeCp2 adsorption and the corresponding unit cell expansion, as determined by XRD.

The diamagnetic nature of both, Zr4+ ions of the MOFs and the Fe2+ cations of FeCp2 avoids the occurrence of paramagnetic line broadening effects in NMR. Therefore, good quality solid-state 1H and 13C MAS-NMR spectra were recorded for both, pristine and FeCp2-loaded MOFs. Therefore, comparison of the 1H signals before and after FeCp2 adsorption allowed us to determine the FeCp2 content of each material and to get valuable information on the location and environment of the adsorbed molecules.

Free FeCp2 shows a 1H NMR signal at 4.4 ppm, and this signal was found to be practically unaltered when FeCp2 was adsorbed on various MOFs: e.g., in MOF-5 (4.2 ppm) or MOF-177 (4.1 ppm). Conversely, Figure 2 shows the 1H MAS-NMR spectrum of FeCp2@UiO-66, in which a broad signal appears at 8.52 ppm, corresponding to the benzene ring protons of terephthalate, together with two additional signals at 5.58 and 2.30 ppm, not present in the parent sample and that we attribute to adsorbed FeCp2. Analogously, two signals were also observed in the 13C spectrum of FeCp2@UiO-66, at 68.65 and 66.49 ppm (see inset in Figure 2), whereas pure FeCp2 showed only one signal at 69.59 ppm.

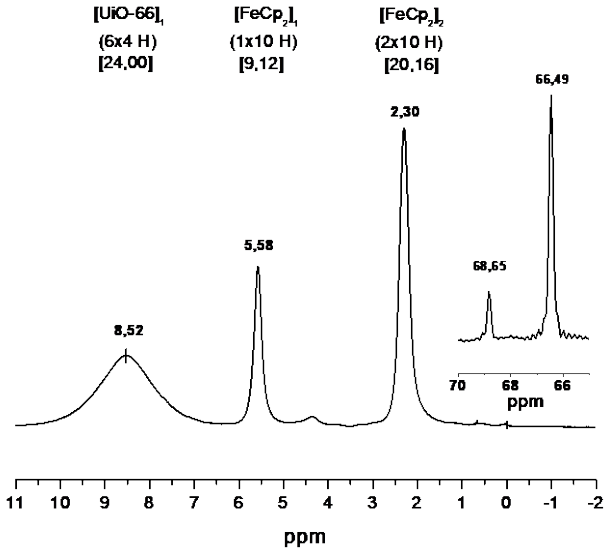

Figure 2. 1H and 13C (inset) solid state MAS-NMR spectra of FeCp2@UiO-66.

Therefore, the effect of the UiO-66 framework on the 1H (and 13C) signals of the cyclopentadienyl protons is remarkable, with respect to previous studies on FeCp2-encapsulated MOFs. This difference can be ascribed to a stronger interaction of FeCp2 with the [Zr6O6] clusters in UiO-66 with respect to the [Zn4O] clusters of MOF-5 and MOF-177, as well as a higher confinement effect inside the UiO-66 pores. In this sense, it is worth mentioning that

tetrahedral and octahedral cavities in UiO-66 are significantly smaller (8 Å and 11 Å internal diameter,[23] respectively) than the cages in the two MOFs mentioned above: 11.8 Å in MOF-5 and 17 Å in MOF-177. From the relative intensities of the 1H signals in FeCp2@UiO-66, the signals at 5.58 ppm and 2.30 ppm should correspond approximately to 1 and 2 FeCp2 molecules per secondary building unit (SBU) of MOF, respectively, for a total number of 3 FeCp2 molecules per SBU. This observation is in perfect agreement with the TGA and ICP-OES data commented above. It is worth noting that the intensity ratio of these two signals with respect to the aromatic protons of UiO-66 (peak envelope at 8.52 ppm) is not fortuitous, but the same ratio has always been consistently obtained in several independent preparations. Since the face centered cubic cell of UiO-66 contains one octahedral and two tetrahedral cavities per SBU, our preliminary interpretation of the 1H MAS-NMR spectra is that the signal at 5.58 ppm should correspond to one molecule of FeCp2 inside the octahedral cavity, while the signal at 2.30 ppm should arise from one FeCp2 molecule in each of the two tetrahedral cavities. The small free openings of the triangular windows connecting both types of cavities should preclude the migration of FeCp2 molecules from one cavity to another at room temperature. Therefore, the 1H NMR spectrum shows different signals for FeCp2 in octahedral and tetrahedral cavities. Note in this sense that according to the TGA curve of FeCp2@UiO-66 (see Fig. S1 in Supporting Information), FeCp2 does not completely desorb from the solid at temperatures below 250ºC, evidencing the diffusion limitations of FeCp2 through the triangular windows of UiO-66. Therefore, according to our preliminary assignment, adsorption of FeCp2 in UiO-66 produces a material that can be formulated as:

$$(\mathrm{FeCp_2})^{Oct}(\mathrm{FeCp_2})_2^{\mathrm{Tet}}@[\mathrm{Zr_6O_6(BDC)_6}]$$

where the superscripts Oct and Tet refer to the location in octahedral and tetrahedral cavities, respectively.

Figure 3 shows the 1H MAS-NMR spectrum of sample FeCp2@UiO-67. Unlike in UiO-66, in this case only one proton signal of adsorbed FeCp2 is observed at 4.02 ppm, whose intensity with respect to the aromatic protons of the MOF (broad and complex signal at ~8.34 ppm) indicates that up to 11 FeCp2 molecules are adsorbed per SBU, in agreement with the data obtained by ICP-OES and TGA. Analogously, only one 13C signal is observed at 68.94 ppm (see inset in Figure 3). In this sense, the results obtained for FeCp2 adsorption in UiO-67 resemble with those previously reported for MOF-5 and MOF-177. However, when the NMR spectrum of FeCp2@UiO-67 was measured at lower temperatures (down to 80ºC), a progressive split of the signal at 4.02 ppm was observed, giving rise to two new peaks at 4.24 and 2.72 ppm with relative intensities of about 5:6 (see Figure 4). A similar split into two signals is also observed in the low-temperature 13C NMR spectra, with new peaks appearing at 68.28 and 66.87 ppm. The changes in both 1H and 13C NMR spectra upon lowering the temperature are completely reversible, and the original single signals in 1H and 13C NMR spectra are recovered once the temperature is raised again.

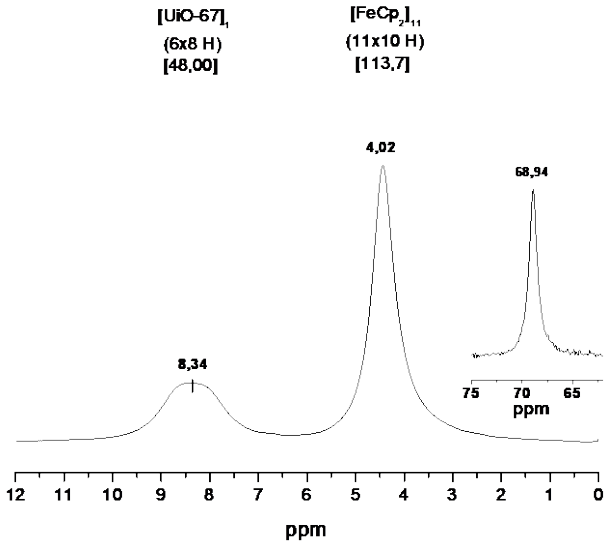

Figure 3. 1H and 13C (inset) solid state MAS-NMR spectra of FeCp2@UiO-67.

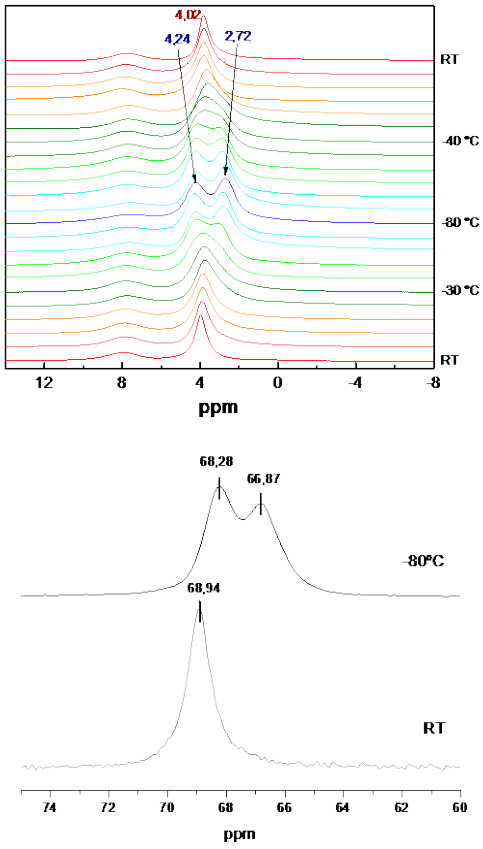

Figure 4. (Top) Variable temperature 1H solid state MAS-NMR spectra of sample FeCp2@UiO-67. (Bottom) Comparison of the 13C solid state MAS-NMR spectra obtained at room temperature and -80ºC.

To interpret these results, we considered that the triangular windows connecting tetrahedral and octahedral cavities in UiO-67 are considerably larger than in UiO-66 (see Figure 1). Therefore, rapid exchange of the FeCp2 from one cavity to another is expected to occur at room temperature, so that the 1H and 13C NMR spectra (Fig. 3) show single averaged signals for FeCp2 in octahedral and tetrahedral cavities. However, when the temperature is lowered, diffusion of

the FeCp2 molecules in the solid is progressively hampered, and two different species can be detected, as in the case of UiO-66. Considering the relative intensities of the 1H signals in Fig. 4, FeCp2@UiO-67 at low temperature (-80ºC) can be formulated as:

$$(FeCp_2)_5^{Oct}(FeCp_2)_6^{Tet}@[Zr_6O_6(BPDC)_6]$$

Thus, up to 5 FeCp2 molecules would be encapsulated inside the larger octahedral cavities of UiO-67, while 3 molecules would be located in each of the two smaller tetrahedral cavities.

Preparation of Pd NPs encapsulated in UiO-66 and UiO-67

In our first attempts to prepare Pd NPs inside UiO-type materials by CVI, adsorption of the Pd precursor (allyl)Pd(Cp) was carried out at room temperature (298 K) for 1 day, under similar conditions to those used for FeCp2 loading. However, in the case of UiO-66 we observed that fast decomposition and uncontrolled reduction of the precursor was taking place, even without requiring UV irradiation. Accordingly, the corresponding electron microscopy images revealed the formation of Pd NPs of 1-2 nm that tend to aggregate into berries of about 20-30 nm, mostly decorating the external surface of the MOF (see Figure 5). Most probably, the well-known Lewis acidity of the [Zr6O6] clusters of UiO-66 is responsible for the uncontrolled decomposition of the precursor.[24-28] Analysis of this material by ICP-OES revealed a final loading of 16.4 wt% Pd. Despite the relatively high metal loading, no additional diffraction lines corresponding to metallic Pd were detected in the corresponding XRD patterns (see Fig. S5 in Supporting Information), which is in agreement with the small size of the individual Pd particles. This sample will be hereafter referred to as Pd298K@UiO-66, were the subscript 298K indicates the temperature used for the adsorption of the Pd precursor.

It is evident that the location of the Pd NPs at the external surface of the MOF ruins the possibility of having shape-selective properties, which was one of the goals of the present study. Therefore, in order to prevent the uncontrolled decomposition of the precursor and deposition of Pd NPs at the external surface of the MOF as much as possible, adsorption experiments were performed at lower temperatures (263 K) and extending the contact time to 7 days to increase the final metal loading. In this way, samples denoted (allyl)PdCp263K@UiO-66 and (allyl)PdCp263K@UiO-67 were prepared. Characterization of these samples by FTIR and 1H and 13C MAS-NMR (see Figures S6-S7 in Supporting Information) allowed us to determine that loading of the organometallic precursor adsorbed in UiO-66 and UiO-67 was about 0.6 and 3 molecules of (allyl)Pd(Cp) per SBU, respectively. Thus, unlike the case of FeCp2, complete filling of the MOF cavities was not attained, due to the diffusion problems of the precursor at such a low temperature.

Formation of Pd NPs inside the MOF pores was achieved by decomposing the adsorbed Pd precursor by UV irradiation (see Experimental Section), yielding the samples that will be hereafter referred to as Pd263K@UiO-66 and Pd263K@UiO-67. According to the elemental analysis by ICP-OES, the final metal loading attained was considerably lower than when the adsorption was carried out at room temperature: 4.7 wt% and 5.7 wt% Pd in UiO-66 and UiO-67 (as compared to 16.4 wt% Pd attained in sample Pd298K@UiO-66). HRTEM images shown in Figure 5 reveal the formation of tiny Pd NPs (1-2 nm), as well as the absence of a significant amount of NPs deposited at the external surface of UiO-67. Meanwhile, a very small fraction of Pd NPs was detected at the external surface of UiO-66, which is probably caused by a higher accumulation of the Pd precursor at the external rims of the crystals due to diffusion limitations.

No significant changes or loss of crystallinity of the MOFs occurred upon loading of the Pd precursor and its photochemical decomposition, as determined by comparison of the XRD patterns before and after the process (Figure S8 in Supporting Information). Likewise, no additional diffraction lines due to metallic Pd were detected. Figure 5 shows a schematic representation of the type and location of the Pd NPs formed in UiO-66 and UiO-67 at the two adsorption temperatures used, together with some representative microscopy images.

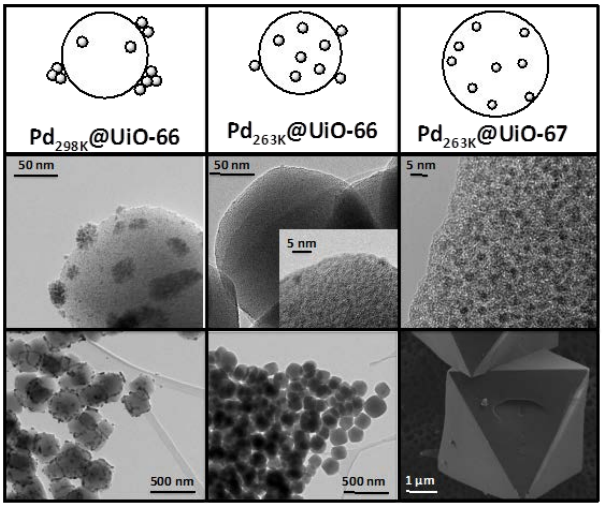

Figure 5. Typical electron microscopy images and schematic representation of the Pd NPs formed in the MOF samples (see text for details).

Selective hydrogenation of ketones to secondary alcohols over Pd@MOF

We selected hydrogenation of carbonyl compounds to test the catalytic properties of the Pd@MOF samples prepared by CVI and the eventual occurrence of shape-selective properties associated to the confinement of the NPs inside the cavities. To this end, we evaluated the reactivity of the materials with two substrates of different steric hindrance: acetophenone (AP) and benzophenone (BP). For the sake of comparison, a commercial hydrogenation catalyst, Pd/C, was used as a model system, lacking any shape selective behavior.

Figure 6 (Top) shows the kinetic curves obtained for AP over the different samples: Pd298K@UiO-66 (with NP mainly at the external surface), Pd263K@UiO-66 and Pd263K@UiO-67 (with NPs preferentially at the internal surface), and the reference Pd/C material (an all-external surface material). In all cases, conversion of AP yielded 1-phenylethanol selectively, while other side products were not detected; e.g., ethylbenzene, 1-cyclohexylethanol or ethylcyclohexane coming from the over-reduction of AP, or styrene coming from water elimination.

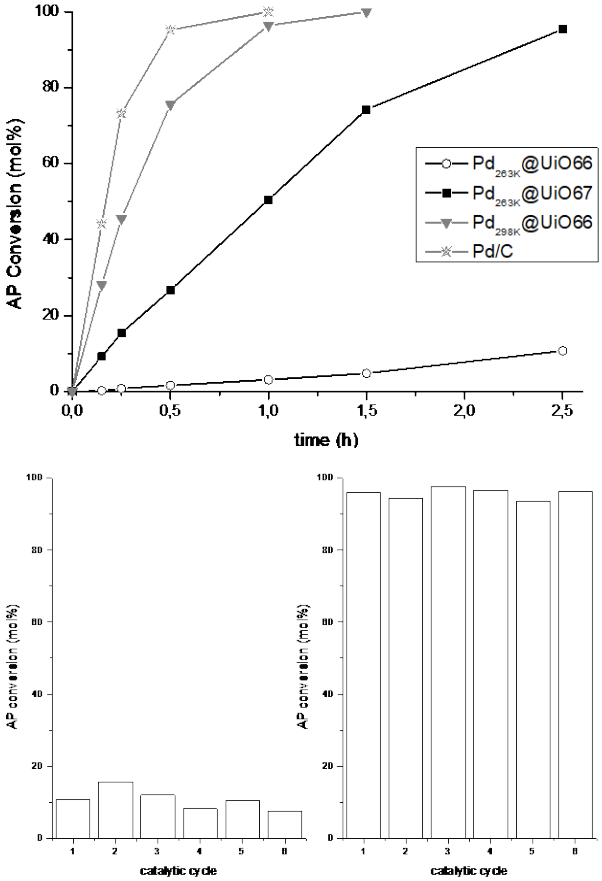

Figure 6. (Top) Time-conversion plot of acetophenone hydrogenation (60ºC, p(H2) = 0.5 MPa) over the Pd catalysts, as indicated. (Bottom) Acetophenone conversion obtained after 2.5 h over Pd263K@UiO-66 (left) and Pd263K@UiO-67 (right) in various consecutive catalytic cycles.

As it can be seen in Fig. 6, clear differences exist in the hydrogenation rates of AP over the various materials, even though the same amount of catalyst (1 mol% Pd) was used in all cases. Thus, it is evident that location of the Pd NPs at the external surface of the catalyst (as in Pd/C and Pd298K@UiO-66) results in a high hydrogenation rate of AP to phenylethanol. On the contrary, the catalytic performance of Pd263K@UiO-66 is very low, due to evident diffusion limitations of AP to the internal surface of UiO-66 (where most of the NPs are located), through the ≈ 6 Å triangular pores. In a separate experiment, we checked that the poor activity of Pd263K@UiO-66 for AP reduction was not due to a low sample quality, since this material was found to hydrogenate 1-hexene (which should have no diffusion limitations) completely after 12 h under similar conditions. Finally, the performance of Pd263K@UiO-67 was found to be intermediate between that of the two Pd@UiO-66 materials studied, as expected in view of the wider pore openings (Ø ≈ 7 Å) with respect to UiO-66.

Pd263K@UiO-66 and Pd263K@UiO-67 were found to be stable under the reaction conditions used, and crystallinity loss or Pd leaching were not detected (according to ICP-OES analysis of both the used catalysts and the reaction filtrates). This allowed us to recover the catalysts at the end of the reaction and reuse them for at least 6 cycles without significant changes in their catalytic activity. Meanwhile, FTIR spectra of the solids recovered after the hydrogenation reaction did not show evidences for the eventual formation of Pd-hydride species on the Pd NPs during the hydrogenation reactions. Figure 6 (bottom part) shows the AP conversion obtained after 2.5 h of reaction in the consecutive catalytic cycles for samples

Pd263K@UiO-66 and Pd263K@UiO-67. It is relevant to note that practically the same high yields were always obtained over Pd263K@UiO-67, while the activity of Pd263K@UiO-66 remained also constant and did not increase with the repeated use. Note that an increased hydrogenation performance of Pd263K@UiO-66 with use could be indicative for aggregation of the metal NPs and migration to the external surface of the MOF particles, resulting in a loss of the shape-selective properties that avoid AP hydrogenation, which is clearly not the case. Thus, although electron microscopy (see Fig. S9) revealed a significant increase of larger metal aggregates (ca. 4-5 nm) in the material recovered after 6 cycles, our catalytic results would suggest that most of these larger particles are located at the internal surface of the MOF and inaccessible to AP. Note that formation of these larger metal particles would probably require a partial destruction of the MOF skeleton to create big (fused) cavities to accommodate them. In any case, it is worth mentioning that our estimation is that large Pd NPs should only account for roughly 10% of the total Pd in sample Pd263K@UiO-66, while the rest of Pd is still in the form of small NPs of 1-2 nm at the internal surface of the MOF.

In order to confirm the existence of shape-selective properties in the Pd@UiO-type material, hydrogenation of a bulkier ketone, BP, was also carried out. The results obtained with the different catalysts are shown in Figure 7.

As in the case of AP hydrogenation, Pd/C was the best performing catalyst also for BP hydrogenation, followed by Pd298K@UiO-66 (having Pd NPs at the external surface). We also observed that BP hydrogenation was very slow over Pd263K@UiO-67, while it practically did not take place when Pd263K@UiO-66 was used as catalyst. These results reflect the higher diffusion problems of BP with respect to AP, even in the UiO-67 material, thus hampering their interaction with the encapsulated Pd NPs.

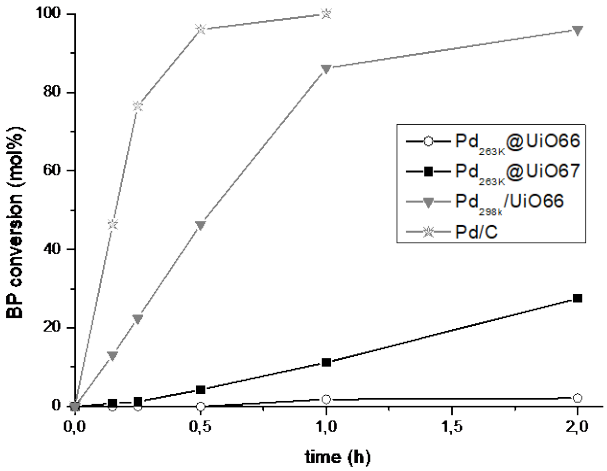

Figure 7. Time-conversion plot of benzophenone hydrogenation (60ºC, p(H2) = 0.5 MPa) over the Pd catalysts.

From the kinetic data shown in Figures 6 and 7, the corresponding turnover frequencies, TOFs, for hydrogenation of AP and BP were calculated for each catalyst, and the results are shown in Table 1.

Table 1. Turnover frequencies (TOF) obtained for AP and BP hydrogenation over the Pd-containing materials.

Catalyst	$TOF_{AP}(h^{-1})$	$TOF_{BP}(h^{-1})$	TOF_{AP}/TOF_{BP}
Pd/C	263.4	279.5	0.94
Pd_{298K}@UiO-66	168.6	78.9	2.12
Pd_{263K}@UiO-67	55.42	8.6	6.44
Pd_{263K}@UiO-66	3.2	-	-

As it can be observed, both molecules are reduced practically at the same rate over Pd/C (TOFAP/TOFBP = 0.94), while clear differences are observed when Pd298K@UiO-66 was used as catalyst (TOFAP/TOFBP = 2.12). Since this sample only contains NPs at the external surface of the MOF and shape-selective properties are thus not expected, the different reduction rate of AP and BP over this material provides an estimation of the intrinsic relative reactivity of the two molecules over Pd-supported UiO-type materials, which should depend mostly on the adsorption rate of both substrates (and desorption of the corresponding products) on the Pd NPs. However, when the reaction was carried out in the presence of Pd263K@UiO-67, a further decrease of the relative hydrogenation rate of BP with respect to AP was observed (TOFAP/TOFBP = 6.44), that should reflect the slower diffusion of BP through the channel system of UiO-67; or in other words, the shape-selective properties introduced by the MOF framework. The low activity observed for AP and BP reduction over Pd263K@UiO-66 makes it difficult to provide accurate values of relative TOFs, due to the high error in the calculations. Thus, in spite of the obvious decrease of the hydrogenation rate of BP with respect to AP over this material, it is risky to determine whether this is due only to the relative intrinsic reactivity of the two compounds, or if a shape-selective process is also involved. Nevertheless, quantification of the eventual shape-selective properties of Pd263K@UiO-66 in terms of AP and BP hydrogenation rate constant ratio would contain an important error, thus being practically meaningless.

Conclusions

Gas phase loading of FeCp2 in the MOFs UiO-66 and UiO-67 has revealed insightful information concerning the host-guest chemistry of these compounds. A detailed study by a multi-technique approach (XRD, TGA, ICP-OES, FTIR, UV-Vis and 1H- and 13C MAS-NMR) allowed us to conclude that up to 3 and 11 FeCp2 molecules per [Zr6O6] cluster can be incorporated in UiO-66 and UiO-67, respectively. Variable-temperature solid state MAS-NMR indicates the existence of two different FeCp2 species, depending on the type of cavity (tetrahedral or octahedral) in which FeCp2 is incorporated. These two species would be highly mobile and rapidly exchangeable in UiO-67 at room temperature, while they would remain trapped in the structural cavities of the material as the temperature is decreased to -80ºC.

The organometallic compound (allyl)Pd(Cp) is a suitable precursor for preparing Pd NPs inside UiO-66 and UiO-67 by gas phase infiltration, provided the adsorption is carried out below room temperature (viz. -10ºC) to avoid uncontrolled decomposition of the precursor and deposition of the NPs at the external surface of the MOF.

Controlled generation of Pd NPs inside the structural cavities of UiO-66 and UiO-67 endows the resulting materials with shape-selective hydrogenation properties, as we

demonstrate for the reduction of acetophenone and benzophenone to the corresponding secondary alcohols.

Experimental Section

Starting Materials. All chemicals were purchased from Sigma-Aldrich or Alfa Aesar and are used without further purification. Manipulations were carried out under Argon atmosphere using standard Schlenk-line and glovebox techniques. All the solvents were purified, dried using an automatic catalytic Solvent Purification System (MBraun, Garching). Ferrocene was purchased from Alfa Aesar and further purified by sublimation. The [Pd(η3-C3H5)(η5-C5H5)] precursor was synthesized according to literature procedure.[29]

Analytical characterization. Elemental analysis (Fe and Pd) was performed on an AAS apparatus by Vario of type 6 (1998). C, H, N analyses were carried out using a Vario CHNSO EL (1998) instrument. Infrared spectra were measured (inside a glovebox) on a Bruker Alpha-P FT-IR instrument in the ATR geometry with a diamond ATR unit. Solid-state 1H and 13C CP-MAS-NMR spectra recorded at room temperature were measured with a Bruker DSX 400 MHz instrument in ZrO2 rotors (diameter = 2.5 mm) with a rotational frequency of 20 kHz, while high and low temperature 1H and 13C spectra were recorded with a 4 mm ZrO2 rotor with a rotational frequency of 10 kHz. Thermo gravimetric analyses (TGA) studies were carried out using a Seiko TG/DTA 6300S11 instrument at a heating rate of 5°C/min in a temperature range from 30-1000 °C at atmospheric pressure under N2 flow (99.9999%; flow rate=300 mL/min). The BET surface area measurements were carried out using N2 gas with a prior degassing step of the samples at 100 °C for 12 h under vacuum. N2 adsorption measurements were performed on a Quantachrome Autosorp-1 MP instrument using optimized protocols. Powder XRD patterns (PXRD) of the samples were recorded with a D8-Advance Bruker AXS diffractometer with Cu Ka-radiation (λ=1.5418Å) in θ–2θ geometry and with a position-sensitive detector. The experimental set-up was in the capillary mode. For data accumulation, the samples were filled under inert gas (glove-box) into capillaries which were then sealed. HRTEM images were obtained with a Jeol JEM 2100F instrument and a Tecnai G2 F20, both operating at 200 kV. DR-UV-Vis spectra were obtained with a Varian Cary 5000 spectrophotometer equipped with a Praying Mantis diffuse accessory.

Synthesis of UiO-66, UiO-66-NH2 and UiO-67. All syntheses were performed according to Schaate et al.[30] Briefly, in 1 L teflon-capped glass flasks, ZrCl4 (1.2 g, 5.14 mmol for UiO-66 and UiO-66-NH2; and 1.8 g, 7.71 mmol for UiO-67) and 30 equivalents of modulator (acetic acid for UiO-66 and UiO-66-NH2; or benzoic acid for UiO-67) were dissolved in 300 mL DMF by using ultrasound for about 10 min. The linker was added to the clear solution in an equimolar ratio with regard to ZrCl4 (terephthalic acid, H2BDC, 0.855 g, for UiO-66; aminoterephthalic acid, H2ATA, 0.930 g, for UiO-66-NH2; or 4,4'-biphenyldicarboxylate, H2BPDC, 1.875 g, for UiO-67) and dissolved or, in the case of H2BPDC, dispersed by ultrasound for about 10 min. The capped flasks were kept in an oven at 120 ºC under static conditions. After 24 h, the solutions were cooled down to room temperature and the precipitates were isolated by centrifugation. The solids were washed three times with fresh DMF (20 mL). After that the solids were left standing at room temperature for periods of 6 h with fresh DMF (3 times x 20 mL) and CHCl3 (3 times x 20 mL). The centrifugated solids were dried under reduced pressure at RT. Finally, the materials were placed in tubular Schlenks under high vacuum at 300 ºC during 24 h. The activated materials were kept inside of a glovebox.

Gas phase loading of ferrocene. Gas phase loading of FeCp2 was performed using the same method as previously described for MOF-5.[9] Briefly, 100 mg of MOF previously dehydroxylated and 200 mg of FeCp2 were placed in separate recipients inside a Schlenk tube under inert atmosphere (Ar). The system was evacuated at high vacuum (10-6 mbar) and kept for one week at 393 K under static conditions to allow FeCp2 to freely diffuse inside the MOF pore system. At the end of the loading process, excess FeCp2 was deposited on the tube walls, thus evidencing that the amount of FeCp2 used was enough to completely saturate the MOFs.

Preparation of palladium nanoparticles. Gas phase loading of the organometallic precursor [Pd(□3-C3H5)(□5-C5H5)], hereafter (allyl)Pd(Cp), was performed with the conditions described in the text. Reduction of the precursor to obtain Pd nanoparticles was achieved by irradiation of the MOF-loaded samples placed inside quartz Schlenk tubes under inert atmosphere using a 500 W mercury lamp (□=264 nm) overnight, followed by evacuation at high vacuum for several hours, first at RT and finally at 100ºC.

Catalytic hydrogenation of ketones. Hydrogenation of ketones, acetophenone and benzophenone (0.1 mmol), was carried out at 60ºC inside 2 mL reactors pressurized at 5 bars with H2, with isopropanol (1 mL) as solvent. The amount of catalyst used in each case was adjusted to have a 1 mol% Pd with respect to the carbonyl compound, corresponding to 2 and 3 mg of solid in the case of Pd263K@UiO-66 and Pd263K@UiO-67, respectively. The reaction products were analyzed by GC and GC-MS using hexadecane as external standard. After each cycle, the solid catalysts were recovered by filtration and thoroughly washed with acetone and dried at 60ºC overnight before reuse. The crystallinity of the recovered material was determined by XRD and compared with that of the fresh material.

Acknowledgements

Financial support from the Consolider-Ingenio 2010 (project MULTICAT), the Severo Ochoa program, and the Spanish Ministry of Science and Innovation (project MAT2011-29020-C02-01) is gratefully acknowledged. C.R. is grateful for a graduate student fellowship awarded by the Cluster of Excellence RESOLV (EXC 1069) funded by the Deutsche Forschungsgemeinschaft (DFG). This project has received funding from the European Union's Horizon 2020 research and innovation programme under the Marie Skolodowska-Curie grant agreement No 641887.

Keywords: Metal Organic Frameworks • Heterogeneous catalysis • Chemical Vapor Infiltration • Shape-selective hydrogenation • Palladium nanoparticles

[1] A. Corma, H. Garcia, F. X. Llabrés i Xamena, Chem. Rev. 2010, 110, 4606.

[2] D. Farrusseng, S. Aguado, C. Pinel, Angew. Chem., Int. Ed. 2009, 48, 7502.

[3] J. Gascon, A. Corma, F. Kapteijn, F. X. Llabrés i Xamena, ACS Catal. 2014, 4, 361.

[4] F. X. Llabrés i Xamena, J. Gascon (eds.), Metal Organic Frameworks as Heterogeneous Catalysts, The Royal Society of Chemistry, Cambridge, 2013.

[5] B. Li, H. Wang, B. Chen, Chem. Asian. J. 2014, 9, 1474.

[6] J.-R. Li, R. J. Kuppler, H. Zhou, Chem. Soc. Rev. 2009, 38, 1477.

[7] L. E. Kreno, K. Leong, O. K. Farha, M. D. Allendorf, R. P. Van Duyne, J. T. Hupp, Chem. Rev. 2012, 112, 1105.

[8] D. Esken, S. Turner, O. I. Lebedev, G. Van Tendeloo, R. A. Fischer, Chem. Mater. 2010, 22, 6393.

[9] S. Hermes, M. K. Schroter, R. Schmid, L. Khodeir, M. Muhler, A. Tissler, R. W. Fischer, R. A. Fischer, Angew. Chem., Int. Ed. 2005, 44, 6237.

[10] M. Meilikhov, K. Yusenko, D. Esken, S. Turner, G. Van Tendeloo, R. A. Fischer, Eur. J. Inorg. Chem. 2010, 3701.

[11] F. Schroeder, D. Esken, M. Cokoja, M. W. E. van den Berg, O. I. Lebedev, G. van Tendeloo, B. Walaszek, G. Buntkowsky, H. H. Limbach, B. Chaudret, R. A. Fischer, J. Am. Chem. Soc. 2008, 130, 6119.

[12] C. Rösler, D. Esken, C. Wiktor, H. Kobayashi, T. Yamamoto, S. Matsumura, H. Kitagawa, R. A. Fischer, Eur. J. Inorg. Chem. 2014, 5514.

[13] M. Muller, S. Hermes, K. Kaehler, M. W. E. van den Berg, M. Muhler, R. A. Fischer, Chem. Mater. 2008, 20, 4576.

[14] M. Muller, X. N. Zhang, Y. M. Wang, R. A. Fischer, Chem. Commun. 2009, 119.

[15] C. Rösler, R. A. Fischer, CrystEngComm 2015, 17, 199.

[16] J. Hermannsdorfer, M. Friedrich, N. Miyajima, R. Q. Alburquerque, S. Kummel, R. Kempe, Angew. Chem., Int. Ed. 2012, 51, 11473.

[17] F. G. Cirujano, F. X. Llabres i Xamena, A. Corma, Dalton Trans. 2012, 41, 4249.

[18] F. G. Cirujano, A. Leyva-Pérez, A. Corma, F. X. Llabrés i Xamena, ChemCatChem 2013, 5, 538.

[19] Z. Guo, C. Xiao, R. V. Maligal-Ganesh, L. Zhou, T. W. Goh, X. Li, D. Tesfagaber, A. Thiel, W. Huang, ACS Catal. 2014, 4, 1340.

[20] X. Li, Z. Guo, C. Xiao, T. W. Goh, D. Tesfagaber, W. Huang, ACS Catal. 2014, 4, 3490.

[21] W. Zhang, G. Lu, C. Cui, Y. Liu, S. Li, W. Yan, C. Xing, Y. R. Chi, Y. Yang, F. Huo, Adv. Mater. 2014, 26, 4056.

[22] L. Chen, H. Chen, R. Luque, Y. Li, Chem. Sci. 2014, 5, 3708.

[23] N. A. Ramsahye, J. Gao, H. Jobic, P. L. Llewellyn, Q. Yang, A. D. Wiersum, M. M. Koza, V. Guillerm, C. Serre, C. L. Zhong, G. Maurin, J. Phys. Chem. C 2014, 118, 27470.

[24] F. G. Cirujano, A. Corma, F. X. Llabrés i Xamena, Catal. Today 2014, DOI: 10.1016/j.cattod.2014.08.015.

[25] F. G. Cirujano, A. Corma, F. X. Llabrés i Xamena, Chem. Eng. Sci. 2015, 124, 52.

[26] F. Vermoortele, R. Ameloot, A. Vimont, C. Serre, D. De Vos, Chem. Commun. 2011, 47, 1521.

[27] F. Vermoortele, B. Bueken, G. Le Bars, B. Van de Voorde, M. Vandichel, K. Houthoofd, A. Vimont, M. Daturi, M. Waroquier, V. Van Speybroeck, D. E. de Vos, J. Am. Chem. Soc. 2013, 135, 11465.

[28] F. Vermoortele, M. Vandichel, B. Van de Voorde, R. Ameloot, M. Waroquier, V. Van Speybroeck, D. E. de Vos, Angew. Chem., Int. Ed. 2012, 51, 4887.

[29] W. R. McClellan, H. H. Hoehn, H. N. Cripps, E. L. Muetterties, B. W. Howk, J. Am. Chem. Soc. 1961, 83, 1601.

[30] A. Schaate, P. Roy, A. Godt, J. Lippke, F. Waltz, M. Wiebcke, P. Behrens, Chem. Eur. J 2011, 17, 6643.

Entry for the Table of Contents

Encapsulation of Pd nanoparticles inside the pores of UiO-66 and UiO-67 by chemical vapor infiltration leads to shape-selective catalysts, as shown for the hydrogenation of carbonyl compounds of different steric hindrance.